ATLAS NOTE

ATLAS-CONF-2013-024

March 7, 2013
Minor Revision: April 9, 2013

Search for direct production of the top squark in the all-hadronic $t\bar{t}+E_{\mathrm{T}}^{\mathrm{miss}}$ final state in 21 fb^{-1} of p-p collisions at $\sqrt{s}=8$ TeV with the ATLAS detector

The ATLAS Collaboration

Abstract

The results of a search for direct pair production of scalar partners of the top quark in 20.5 fb^{-1} of pp collisions at $\sqrt{s}=8$ TeV using the ATLAS detector at the LHC are reported. The top squarks are assumed to decay exclusively into a top quark and the lightest supersymmetric particle. The search is conducted in events with large missing transverse momentum and six or more jets, targeting the fully-hadronic top final state. Results are interpreted in a R-parity conserving minimal supersymmetric scenario of direct top squark pair production. Top squarks in this model with masses between 320 and 660 GeV are excluded at 95% CL for a nearly massless LSP. For a LSP mass of 150 GeV the exclusion interval is between 400 and 620 GeV. The result significantly extends previous limits in the all-hadronic final state and excludes top squarks up to higher masses than in previous searches.

In the version of March 7, Fig. 4 left was missing the contribution from Z+jets. This plot has now been replaced. Only this plot was affected. The analysis and the results remain unchanged.

ATLAS-CONF-2013-024
09/04/2013

1 Introduction

The recent observation at the Large Hadron Collider (LHC) [1] of a particle consistent with the Standard Model (SM) Higgs Boson [2,3] has brought renewed attention to the gauge hierarchy problem [4–7]. Supersymmetry (SUSY) [8–16] provides an extension of the SM which resolves the hierarchy problem [17–22] by introducing supersymmetric partners of the known bosons and fermions. The dominant contribution to the divergence of the Higgs boson mass arises from loop diagrams involving the top quark; these can be largely canceled if the scalar partner of the top quark (top squark) has a mass below approximately the TeV scale [23,24]. The two top squark states ($\tilde{t}_L$ and $\tilde{t}_R$), superpartners corresponding to the left- and right-handed top quarks, mix to form the two mass eigenstates, $\tilde{t}_1$ and $\tilde{t}_2$; due to the large top Yukawa coupling, the mixing can be large, resulting in a significant mass-splitting between the lighter (designated as $\tilde{t}_1$) and heavier top squarks. In the framework of the R-parity conserving minimal supersymmetric extension of the SM (MSSM) [17,25–28], SUSY particles are produced in pairs and the lightest supersymmetric particle (LSP) is stable, providing a possible candidate for dark matter. The undetected LSP results in missing transverse momentum, whose magnitude is denoted as $E_{\mathrm{T}}^{\mathrm{miss}}$.

This note reports on a search with the ATLAS detector for direct $\tilde{t}_1$ pair production, extending the analysis described in Ref. [29]. The search utilizes the full 2012 dataset, collected at a pp center-of-mass energy of $\sqrt{s} = 8$ TeV and corresponding to an integrated luminosity of 20.5 fb^{-1}. The search is optimized under the assumption that each top squark decays exclusively to a top quark and the LSP, and is targeted towards top quark decay in the all-hadronic channel. The final state for this search is therefore six or more jets and $E_{\mathrm{T}}^{\mathrm{miss}}$. The search is nearly insensitive to the details of the top quark polarization, and hence to the mixture of $\tilde{t}_L$ and $\tilde{t}_R$ in the mass eigenstates. Previous searches for direct top squark production at center-of-mass energies of 7 and 8 TeV have been reported by the ATLAS [30–34] and CMS [35–38] collaborations.

2 Simulated event samples and SUSY signal modeling

Samples of simulated events are used for the description of the background and to model the SUSY signal. The main backgrounds to this search arise from $t\bar{t}$ production where one top decays semi-leptonically (with the lepton, primarily taus, mis-identified as a jet), $Z(\rightarrow \nu\bar{\nu})$ plus heavy-flavor jets, and the irreducible background from $t\bar{t}$ +$Z(\rightarrow \nu\bar{\nu})$. Other background processes which are considered are multijets, Z plus light-flavor jets, W plus light- and heavy-flavor jets, single-top, $t\bar{t}$ +W, $t\bar{t}$ +WW, and diboson production.

Top quark pair production, followed by the leptonic decay of one of the top quarks, is simulated with POWHEG [39] while MC@NLO [40,41] is used to model top quark pair production in the all-hadronic channel, as well as single-top production in the s- and Wt channels. ACER MC [42] is used for single-top production in the t-channel. SHERPA [43] is used for W+jets and Z+jets production (including heavy-flavor jets) as well as for diboson (WW, ZZ and WZ) production. MADGRAPH [44] is used for $t\bar{t}+Z$, $t\bar{t}+W$ and $t\bar{t}+WW$ production.

The fragmentation/hadronization for the MC@NLO samples are performed with HERWIG [45], using JIMMY [46] for the underlying event, while PYTHIA [47] is used for samples generated with POWHEG, MADGRAPH and ACER MC. The parton density function (PDF) sets used for the SM backgrounds are: CT10 [48] for the MC@NLO, POWHEG and SHERPA samples, and CTEQ6L1 [49] for the MADGRAPH and ACER MC samples. The underlying event tunes are the ATLAS AUET2B [50] for POWHEG, ACER MC and MADGRAPH samples and AUET2 [51] for the

MC@NLO sample.

For the initial comparison with data, all SM background cross sections are normalized to the results of higher-order calculations when available. The theoretical cross sections for W+jets and Z+jets are calculated with DYNNLO [52] with the MSTW 2008 NNLO [53] PDF set. The same K-factor, i.e. the ratio of next-to-next-leading-order (NNLO) to leading-order cross sections, is applied to the production of W/Z in association with heavy-flavor jets. The inclusive $t\bar{t}$ cross section is calculated with HATHOR 1.2 [54] using MSTW 2008 NNLO PDFs. The production of $t\bar{t}$ in association with W/Z are normalized to NLO cross sections [55,56]. Single-top cross sections are taken from MC@NLO. For the diboson cross sections, MCFM [57] with the MSTW 2008 NLO PDFs is used. The $t\bar{t}+WW$ cross section is taken from MADGRAPH.

The signal samples are generated using HERWIG++ [58]. The mixing matrices for the top squark and for the neutralinos are chosen such that the top quark produced in the decay has a right-handed polarization in 95% of the decays. A subset of signal samples are generated with top squarks corresponding to the left-handed top quark in order to assess the impact on the signal acceptance. Signal cross sections are calculated to NLO in the strong coupling constant, adding the resummation of soft gluon emission at next-to-leading-logarithmic accuracy (NLO+NLL) [59–61]. The nominal cross section and the uncertainty are taken from an envelope of cross section predictions using different PDF sets and factorization and renormalization scales, as described in Ref. [62].

The detector simulation [63] is performed using GEANT4 [64] or a fast simulation framework where the showers in the electromagnetic and hadronic calorimeters are simulated with a parametrized description [65] and the rest of the detector simulated with GEANT4. All samples are produced with a range of simulated minimum-bias interactions overlaid on the hard-scattering event to account for multiple pp interactions in the same bunch crossing (pile-up). The overlay also treats the impact of pile-up from bunch crossings other than the one in which the event occurred. Corrections are applied to the simulated samples to account for differences between data and simulation for the lepton trigger and reconstruction efficiencies, momentum scale and resolution, and for the efficiency and mis-tag rates for b-quark tagging.

3 Trigger and data collection

The ATLAS detector [1] has been described elsewhere [66,67]. The data used in this analysis were collected from the end of March through mid-December 2012 during which the instantaneous luminosity of the LHC reached $7.7 \times 10^{33}\text{cm}^{-2}\text{s}^{-1}$. The average number of interactions per bunch crossing ranged from approximately 5 to 40 during the run, with an average of about 21. After the application of beam, detector, and data-quality requirements, the total integrated luminosity is 20.5 fb^{-1}.

The data were collected using several triggers. For the top squark search itself, a missing transverse energy trigger was used. This trigger bases the bulk of its rejection on the vector sum of transverse energies deposited in projective trigger towers (each with a size of approximately $\Delta\eta \times \Delta\phi \sim 0.1 \times 0.1$ for $|\eta| < 2.5$ and larger and less regular in the more forward regions). A more refined calculation based on the vector sum of all calorimeter cells above threshold is made at a later stage in the trigger processing. The trigger required $E_{\text{T}}^{\text{miss}} > 80$ GeV, and is

[1] ATLAS uses a right-handed coordinate system with its origin at the nominal interaction point (IP) in the centre of the detector and the z-axis along the beam pipe. The x-axis points from the IP to the centre of the LHC ring, and the y axis points upward. Cylindrical coordinates (r,ϕ) are used in the transverse plane, ϕ being the azimuthal angle around the beam pipe. The pseudorapidity is defined in terms of the polar angle θ as $\eta = -\ln\tan(\theta/2)$.

fully efficient for offline calibrated $E_{\mathrm{T}}^{\mathrm{miss}} > 150$ GeV, for events passing the jet multiplicity and p_{T} requirements described in Section 5.

Data samples enriched in the major sources of background were collected with electron and muon triggers. The electron trigger selects events based on the presence of clusters in the electromagnetic calorimeter, with a shower shape consistent with that of an electron and a matching track in the tracking system. The transverse energy threshold at the trigger level was 24 GeV (12 GeV) for single (double) electrons. Electron isolation requirements at the trigger level were as follows. The transverse energy in the section of the hadronic calorimeter behind the cluster was required to be less than 1 GeV, and the scalar sum of the p_{T} of tracks within a cone of radius $\Delta R = \sqrt{(\Delta\eta)^2 + (\Delta\phi)^2} = 0.2$ around the electron (excluding the electron itself) was required to be less than 10% of the electron E_{T}. In order to recover some of the efficiency for high-p_{T} electrons, events were also collected with a single-electron trigger with looser shower shape requirements, and no isolation requirements, but with a E_{T} threshold of 60 GeV. The muon trigger selects events containing one or more muon candidates based on tracks identified in the muon spectrometer and inner detector. For the single-muon trigger, the p_{T} threshold was 24 GeV, and the scalar sum of the p_{T} of tracks within a cone of radius $\Delta R = 0.2$ around the muon (excluding the muon itself) was required to be less than 12% of the muon p_{T}. To recover some of the efficiency for higher p_{T} muons, events were also collected with a single-muon trigger with a p_{T} threshold of 36 GeV with no isolation requirement. The di-muon trigger required one muon above a p_{T} threshold of 18 GeV with a second muon above 8 GeV, both without requirements on isolation.

Jet triggers were used to collect data samples for the estimation of the multijet and fully-hadronic $t\bar{t}$ backgrounds. The jet p_{T} thresholds ranged from 55 to 460 GeV. In order to stay within the bandwidth limits of the trigger system, only a fraction of events passing these triggers were recorded to permanent storage.

4 Object reconstruction

The reconstructed primary vertex [68] is required to be consistent with the beam spot envelope and to have at least five associated tracks; when more than one such vertex is found, the vertex with the largest summed $|p_{\mathrm{T}}|^2$ of the associated tracks is chosen.

Electrons, muons and jets are selected in two stages. Electrons are reconstructed from energy clusters in the electromagnetic calorimeter matched to a track in the inner detector [69]. Pre-selected electrons are required to have $|\eta| < 2.47$ and pass a variant of the "loose" selection defined in Ref. [69], re-optimized for 2012 data. Pre-selected electrons are further required to have $p_{\mathrm{T}} > 10$ GeV. Muons are identified either as a combined track in the muon spectrometer and inner detector systems, or as an inner detector track matched with a muon spectrometer segment [70, 71]. Pre-selected muons are required to have $|\eta| < 2.4$ and $p_{\mathrm{T}} > 10$ GeV. Jets are reconstructed using the anti-k_t algorithm [72, 73] with a distance parameter $R = 0.4$. Events containing jets arising from detector noise, cosmic rays or other non-collision sources are rejected [74]. Pre-selected jets are required to have $p_{\mathrm{T}} > 20$ GeV and $|\eta| < 4.5$. Since electrons are also reconstructed as jets, pre-selected jets which overlap with pre-selected electrons within a distance $\Delta R = 0.2$ are discarded. The missing transverse momentum is computed as described in Ref. [75], but using the list of pre-selected electrons, muons and jets instead of the defaults. The missing transverse momentum from the tracking system (denoted as $E_{\mathrm{T}}^{\mathrm{miss,track}}$) is computed from the vector sum of the reconstructed tracks with $p_{\mathrm{T}} > 0.5$ GeV and associated with the primary vertex in the event.

For the final selection of signal candidates, jets are required to have $p_{\mathrm{T}} > 35$ GeV and

$|\eta| < 2.8$. Jets with $|\eta| < 2.5$ arising from b-quarks are identified using information about track impact parameters and reconstructed secondary vertices [76]; the b-tagging algorithm is based on a neural network using the output weights of the IP3D, JetFitter+IP3D, and SV1 algorithms (defined in Ref. [77, 78]) as input. The b-tagging requirements are set at an operating point corresponding to an average efficiency of 70% for b-jets in simulated $t\bar{t}$ events, for which the algorithm provides a rejection factor of approximately 150 for light-quark and gluon jets (depending on the p_{T} of the jet) and a rejection of approximately 5 for charm jets.

For the selection of events in background control regions (described in Sec. 6) requiring leptons, the requirements on electrons and muons are tightened. Electrons are required to pass a variant of the "tight" selection of Ref. [69], re-optimized for 2012 data, and must have $|\eta| < 2.47$ and a distance to the closest jet $\Delta R > 0.4$. Electrons are required to satisfy track- and calorimeter-based isolation criteria. The scalar sum of the p_{T} of tracks within a cone of radius $\Delta R = 0.3$ ("track isolation") around the electron (excluding the electron itself) is required to be less than 16% of the electron p_{T}. The scalar sum of the E_{T} of calorimeter energy deposits (corrected for pile-up) within a cone of radius $\Delta R = 0.3$ ("calorimeter isolation") around the electron (again, excluding the electron itself) is required to be less than 18% of the electron p_{T}. The impact parameter of the electron in the transverse plane with respect to the reconstructed event primary vertex is required to be less than five times the expected impact parameter uncertainty while the impact parameter along the beam direction is required to be less than 0.4 mm. Muons are required to have $|\eta| < 2.4$ and $\Delta R > 0.4$ with respect to the closest jet. Further isolation criteria are imposed: both the track and calorimeter isolation are required to be less than 12% of the muon p_{T}. The transverse impact parameter of the muon is required to be less than three times the expected uncertainty; the longitudinal impact parameter is required to be less than 0.4 mm. The lepton p_{T} requirements vary by background control region, as summarized below in Table 1.

5 Event selection

The event selection criteria are listed in Table 1 for the signal selection as well as the background control region (described in Sec. 6).

Events containing fake $E_{\mathrm{T}}^{\mathrm{miss}}$ arising from jets associated with calorimeter noise or non-collision backgrounds [79], or by cosmic-ray muons or poorly reconstructed muons [71, 80] are rejected. Signal events are required to contain no pre-selected electrons and muons with $\Delta R > 0.4$ with respect to the closest pre-selected jet. Six or more jets are then required, of which ≥ 2 must have been b-tagged. The two leading jets are required to have $p_{\mathrm{T}} > 80$ GeV with the remaining jets having $p_{\mathrm{T}} > 35$ GeV. Events with $E_{\mathrm{T}}^{\mathrm{miss}}$ arising from mis-measured jets or from jets containing an undetected semi-leptonically decaying heavy-flavor hadron are rejected by requiring the azimuthal angle ($\Delta\phi$) between the $E_{\mathrm{T}}^{\mathrm{miss}}$ direction and any of the three highest p_{T} jets in the event ($\Delta\phi(\mathrm{jet}, \mathrm{E}_{\mathrm{T}}^{\mathrm{miss}})$) to be greater than 0.2π. Further reduction of such events is achieved by requiring the $E_{\mathrm{T}}^{\mathrm{miss}}$ calculated from the tracking system to be greater than 30 GeV and to have an angular separation $\Delta\phi(E_{\mathrm{T}}^{\mathrm{miss}}, E_{\mathrm{T}}^{\mathrm{miss,track}})$ less than $\pi/3$ radians with respect to the $E_{\mathrm{T}}^{\mathrm{miss}}$ calculated from the calorimeter system. Events containing tau leptons that are reconstructed as jets are rejected by vetoing events containing a non-b-tagged jet with ≤ 4 associated tracks, where the $\Delta\phi$ between the jet and the direction of $E_{\mathrm{T}}^{\mathrm{miss}}$ is less than 0.2π; this requirement is listed as "tau veto" in Table 1. The background from semi-leptonic $t\bar{t}$ background is further reduced by requiring the transverse mass (m_{T}) between the $E_{\mathrm{T}}^{\mathrm{miss}}$ and the b-tagged jet closest in $\Delta\phi$ to the $E_{\mathrm{T}}^{\mathrm{miss}}$ direction ($m_{\mathrm{T}}(b, E_{\mathrm{T}}^{\mathrm{miss}}) = \sqrt{2p_{\mathrm{T}}^{b}E_{\mathrm{T}}^{\mathrm{miss}}(1-\cos(\Delta\phi(\vec{p}_{\mathrm{T}}^{\,b}, \vec{p}_{\mathrm{T}}^{\,\mathrm{miss}})))}$) to be greater than 175 GeV.

	Signal	$t\bar{t}$ **CR**	**Z+jets CR**	**Multijet CR**
Trigger	$E_{\mathrm{T}}^{\mathrm{miss}}$	single electron (muon)	two electron (muon)	$E_{\mathrm{T}}^{\mathrm{miss}}$
N_{lep}	0	1	2	0
p_{T}^{ℓ}	< 10 (10)	> 35 (35)	> 20 (20)	< 10 (10)
$p_{\mathrm{T}}^{\ell_2}$	—	< 10 (10)	> 20 (10)	—
$m_{\ell\ell}$	—	—	81 to 101	—
N_{jet}	≥ 6	≥ 6	≥ 6	≥ 6
p_{T}^{jet}	> 80,80,35,...35	> 80,80,35,...35	> 80,80,35,...35	> 80,80,35,...35
$N_{b\text{-jet}}$	≥ 2	≥ 2	≥ 2	≥ 2
m_{jjj}	80 to 270	0 to 600	80 to 270	—
$E_{\mathrm{T}}^{\mathrm{miss}}$	> 200, 300, 350	> 200, 300, 350	> 70	> 160
$E_{\mathrm{T}}^{\mathrm{miss,track}}$	> 30	> 30	> 30	> 30
$\Delta\phi(E_{\mathrm{T}}^{\mathrm{miss}}, E_{\mathrm{T}}^{\mathrm{miss,track}})$	$< \pi/3$	$< \pi/3$	$< \pi/3$	$> \pi/3$
$m_{\mathrm{T}}(\ell, E_{\mathrm{T}}^{\mathrm{miss}})$	—	40 to 120	—	—
$\Delta\phi(\mathrm{jet}, \mathrm{E}_{\mathrm{T}}^{\mathrm{miss}})$	$> \pi/5$	$> \pi/10$	$> \pi/5$	$< \pi/5$
$m_{\mathrm{T}}(b\text{-jet}, E_{\mathrm{T}}^{\mathrm{miss}})$	> 175	—	> 175	> 175
Tau veto	yes	no	yes	no

Table 1: Overview of the selection criteria for the signal and control (CR) regions in this analysis. The p_{T} selections for leptons are given for electrons (muons). All mass and momentum requirements are in units of GeV. For the multijet CR, the requirements on $\Delta\phi(E_{\mathrm{T}}^{\mathrm{miss}}, E_{\mathrm{T}}^{\mathrm{miss,track}})$ and $\Delta\phi(\mathrm{jet}, \mathrm{E}_{\mathrm{T}}^{\mathrm{miss}})$ are imposed in a logical OR. For the Z+jets CR, the $E_{\mathrm{T}}^{\mathrm{miss}}$-related requirements are shown after having recomputed $E_{\mathrm{T}}^{\mathrm{miss}}$ following the removal of the two leptons.

Finally, the event is required to have two 3-jet systems whose invariant masses are consistent with that of the top quark. To reduce the combinatorics, the three closest jets in the $\eta - \phi$ plane are combined to form one 3-jet system. A second 3-jet system is defined by repeating the procedure. The invariant mass of each of the 3-jet systems is required to be between 80 and 270 GeV. The final discriminating variable between signal and background is $E_{\mathrm{T}}^{\mathrm{miss}}$. Three signal regions (denoted by SRn, where n=1,2,3) are defined, targeting different ranges of the top squark mass, by varying the lower edge of the $E_{\mathrm{T}}^{\mathrm{miss}}$ requirement, SR1: ≥ 200 GeV, SR2: ≥ 300 GeV, and SR3: ≥ 350 GeV.

6 Background estimation

The backgrounds from semi-leptonic $t\bar{t}$ and Z+jets events are estimated by defining two control regions, one for each background; the control region is defined such that the process of interest is dominant. The simulation is normalized to data in that control region, and the simulation is used to extrapolate the background expectation into the signal region. The multijet background is estimated from the data by taking a sample of well-measured multijet events and smearing the jet energies by a jet response function, determined with PYTHIA8 [81] (and cross-checked against the data), separately for light-quark and heavy-flavor jets; this procedure also accounts for the background from all-hadronic $t\bar{t}$ events. All other backgrounds in the signal and in the control regions are estimated entirely from the simulation, using the most accurate theoretical cross sections available.

The control sample for the semi-leptonic $t\bar{t}$ background is defined with requirements similar to those described in Sec. 5 for the top squark signal candidates but with the following differences. The data sample is based on the single-electron or muon trigger. The requirements on the lepton veto, the tau veto and on $m_{\mathrm{T}}(b, E_{\mathrm{T}}^{\mathrm{miss}})$ are removed. The presence of a single lepton (as described in Sec. 4) is required; events with an additional isolated electron or muon with $p_{\mathrm{T}} > 10$ GeV are rejected. The transverse mass between the lepton and $E_{\mathrm{T}}^{\mathrm{miss}}$ is required to be between 40 and 120 GeV. The lepton is then treated as a non-b-tagged jet before imposing the jet and b-tagged jet multiplicity requirements. The requirement on $\Delta\phi$ between the three leading p_{T} jets and $E_{\mathrm{T}}^{\mathrm{miss}}$ is relaxed to be greater than 0.1π. The mass requirements on the two 3-jet systems are relaxed; the minimum requirement is removed, and the maximum is set to 600 GeV. Three control regions are then defined, one for each signal region, with the same $E_{\mathrm{T}}^{\mathrm{miss}}$ requirement as the corresponding signal region. Figure 1 compares several distributions in data and simulation after these requirements for the semi-leptonic $t\bar{t}$ control region corresponding to SR1 ($E_{\mathrm{T}}^{\mathrm{miss}} > 200$ GeV). The normalization of the simulation to the data in the $t\bar{t}$ control region is performed in a fit described in Sec. 7.

The control sample for $Z(\rightarrow \nu\overline{\nu})$ plus heavy-flavor jets background is based on a sample of $Z(\rightarrow \ell\ell)$+jets events (where ℓ denotes either an electron or muon). The events are collected with the dilepton triggers. Exactly two oppositely charged electrons or muons are required with $p_{\mathrm{T}} > 20, 20$ GeV for electrons and $p_{\mathrm{T}} > 20, 10$ GeV for muons. The invariant mass of the dilepton pair is required to be between 81 and 101 GeV. To reduce the $t\bar{t}$ contamination, the events are required to have $E_{\mathrm{T}}^{\mathrm{miss}} < 50$ GeV. The reconstructed dileptons are then removed from the event and the vector sum of their momenta is added to both the calorimeter and track-based $E_{\mathrm{T}}^{\mathrm{miss}}$; after this recalculation of the $E_{\mathrm{T}}^{\mathrm{miss}}$ the events are required to have $E_{\mathrm{T}}^{\mathrm{miss}} > 70$ GeV. The remaining requirements for the top squark signal regions are then applied. Figure 2 shows the distribution of $E_{\mathrm{T}}^{\mathrm{miss}}$ after it has been recomputed, following the removal of the two leptons from the event. Based on the comparison in the control region, the simulation is scaled up by a factor of 1.06 ± 0.35 to match the data.

The multijet (including fully-hadronic $t\bar{t}$) backgrounds are evaluated using the jet-smearing technique described in Ref. [82]. To validate the technique, the smeared samples are compared to data in a region enriched in multijet events. Six or more jets are required, with the same requirements as in the signal search, including the requirement of two or more b-tagged jets. The calorimeter-based (track-based) $E_{\mathrm{T}}^{\mathrm{miss}}$ is required to be greater than 160 (30) GeV. The requirements on the masses of the two 3-jet systems are dropped. One of the signal region requirements on the azimuthal separation $\Delta\phi(\mathrm{jet}, \mathrm{E}_{\mathrm{T}}^{\mathrm{miss}})$ or $\Delta\phi(E_{\mathrm{T}}^{\mathrm{miss}}, E_{\mathrm{T}}^{\mathrm{miss,track}})$ is inverted to enhance the population of mis-measured multijet events, and the smeared sample is normalized to the data. Figure 3 shows the distribution of these two quantities in the multijet control region. The multijet (and fully-hadronic $t\bar{t}$) backgrounds in the signal regions are then evaluated by applying the remaining signal region requirements on the smeared event sample.

The contamination in the control regions from signal events is ignored. From simulation, the contamination is expected to be at most a few percent in the top and multijet control regions and negligible in the Z+jets control region.

7 Systematic uncertainties and background fit

Systematic uncertainties have an impact on the expected background and signal event yields in the control and signal regions. These uncertainties are treated as nuisance parameters in a profile likelihood fit described later in this section. The following systematic uncertainties on the reconstructed objects are taken into account. The jet energy scale (JES) and jet energy res-

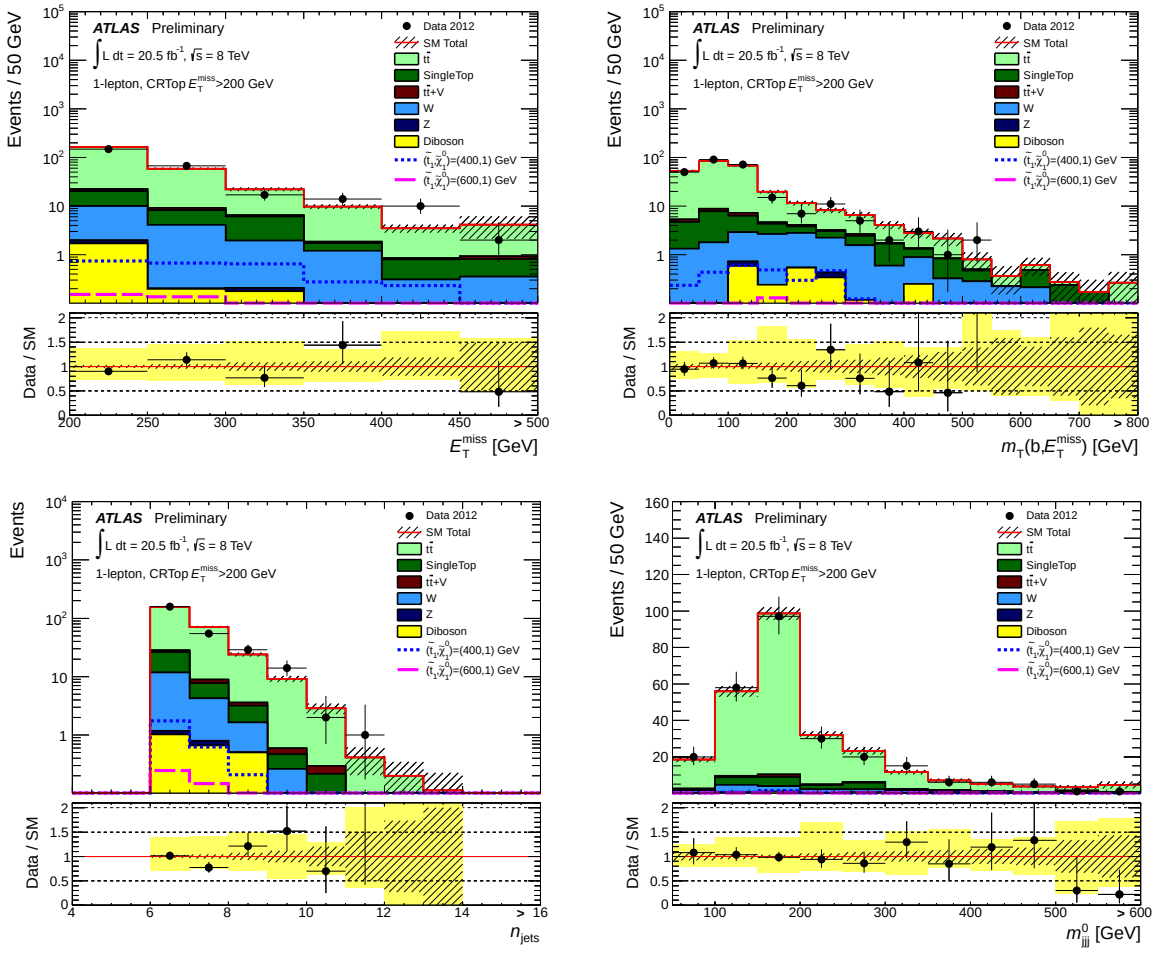

Figure 1: Distributions in the semi-leptonic $t\bar{t}$ control region for SR1 ($E_{\mathrm{T}}^{\mathrm{miss}} > 200$ GeV) after the application of all selection requirements. All kinematic quantities have been recalculated after having treated the lepton as a jet. Top left: $E_{\mathrm{T}}^{\mathrm{miss}}$. Top right: $m_{\mathrm{T}}(b, E_{\mathrm{T}}^{\mathrm{miss}})$. Bottom left: jet multiplicity. Bottom right: invariant mass of the first selected 3-jet system. The stacked histograms show the Standard Model expectation, normalized using the theoretical cross sections. The expectation from two representative signal points (with top squark masses of 400 GeV and 600 GeV and a nearly massless LSP) are shown unstacked. The "Data/SM" plots show the ratio between data and the total Standard Model expectation. The rightmost bin includes all overflows. The grey uncertainty band around the Standard Model expectation shows the statistical uncertainty and the yellow band (shown only for the "Data/SM" plots) shows the combination of statistical and systematic uncertainties.

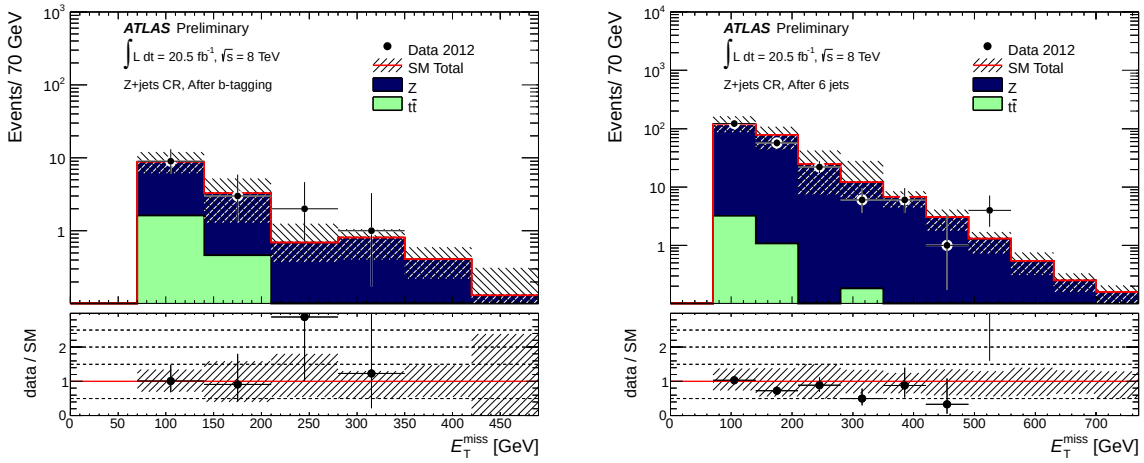

Figure 2: The $E_{\mathrm{T}}^{\mathrm{miss}}$ distribution in the Z+jets control region after all selection requirements (left) and without the requirement on the number of b-tagged jets (right). The $E_{\mathrm{T}}^{\mathrm{miss}}$ has been recomputed after removing the two leptons from the event. The stacked histograms show the Standard Model expectations, normalized using the theoretical cross sections. The "Data/SM" plots show the ratio between data and the total Standard Model expectation. The uncertainty band around the Standard Model expectation is the combination of statistical and systematic uncertainties.

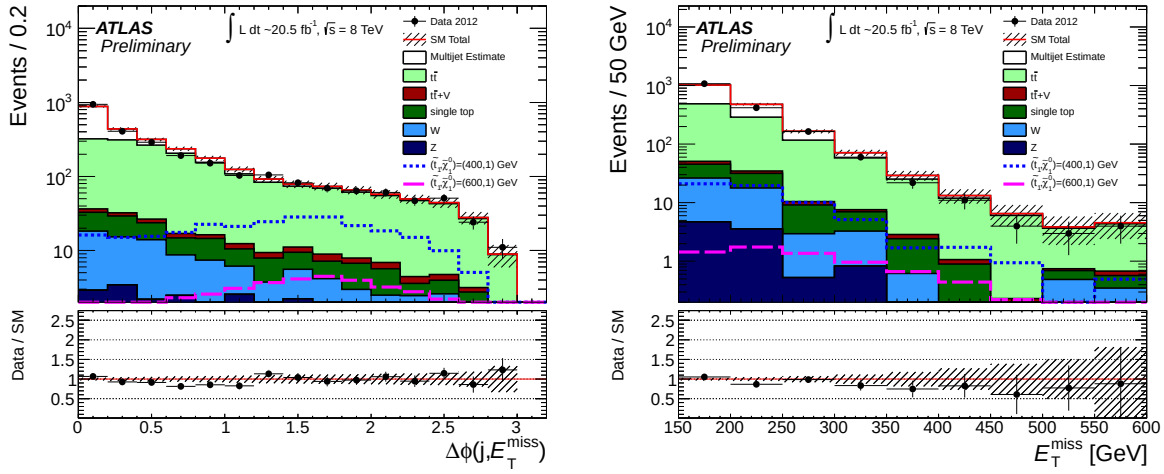

Figure 3: Distributions of $\Delta\phi(\mathrm{jet}, \mathrm{E}_{\mathrm{T}}^{\mathrm{miss}})$ (left) and $E_{\mathrm{T}}^{\mathrm{miss}}$ (right) in the multijet control region. The left plot is shown with neither the requirement on $\Delta\phi(\mathrm{jet}, \mathrm{E}_{\mathrm{T}}^{\mathrm{miss}})$ nor the one on $\Delta\phi(E_{\mathrm{T}}^{\mathrm{miss}}, E_{\mathrm{T}}^{\mathrm{miss,track}})$ applied. The stacked histograms show the Standard Model expectations. The expectation from two representative signal points (with top squark masses of 400 GeV and 600 GeV and a nearly massless LSP) are shown unstacked. The multijet contribution has been normalized to the data after subtraction of the other backgrounds normalized to theoretical cross sections. The "Data/SM" plots show the ratio between data and the total Standard Model expectation. The rightmost bin includes all overflows. The uncertainty band around the Standard Model expectation shows the statistical uncertainty only.

olution (JER) uncertainties are determined from 2012 data, using the techniques described in Refs. [74] and [83]. Uncertainties on the lepton identification, momentum/energy scale and resolution are estimated from samples of $Z \to \ell^+\ell^-$, $J/\psi \to \ell^+\ell^-$ and $W^\pm \to \ell^\pm\nu$ decays in data [69–71]. The uncertainties on the jet and lepton energies are propagated to the $E_{\mathrm{T}}^{\mathrm{miss}}$; an additional $E_{\mathrm{T}}^{\mathrm{miss}}$ uncertainty arising from energy deposits not associated with any reconstructed objects is also included [75]. Uncertainties on the b-tagging efficiency are derived from data samples tagged with muons associated with jets, either utilizing templates of the muon momentum transverse to the closest jet [76] or following the "System8" [84] method [85]. Uncertainties on the light-flavor mis-tag rate are derived by examining tracks with negative impact parameter [86] while charm mis-tag uncertainties are obtained from data samples tagged by reconstructing D^* mesons [87].

Uncertainties from the identification efficiency for jets associated with the reconstructed primary vertex and from the overlay of pile-up in simulated events are both found to be negligible.

Uncertainties in the multijet and fully-hadronic $t\bar{t}$ backgrounds arise from the following uncertainties in the jet-smearing technique: heavy-flavor tagging, Gaussian core and non-Gaussian tail components of the jet response function, and the jet energy scale. The level of agreement between the data and expectation in Fig. 3 indicates that the systematic uncertainty in the background is within 50%. An uncertainty of 100% is assigned to be conservative.

Theoretical uncertainties in the extrapolation of the semi-leptonic $t\bar{t}$ background from the control regions to the signal regions are studied as follows. The impact of missing higher-order diagrams in the matrix element is assessed by varying the renormalization and factorization scales in POWHEG up and down by a factor of two from their nominal values. The effects from varying each of the scales independently are added in quadrature. The impact of modeling uncertainties in fragmentation and hadronization is studied by comparing POWHEG samples interfaced to PYTHIA versus those interfaced to HERWIG/JIMMY. The difference is symmetrized to give the total uncertainty. Uncertainties in the modeling of initial- and final-state radiation (ISR and FSR) are evaluated using several ACER MC samples with differing parton shower settings, constrained by measurement [88]. Half of the difference between the samples is taken as the uncertainty. The impact of treating the lepton in the control region simply as a jet is found to be negligible. For the Z+jets background, an uncertainty on the extrapolation from control region to signal region is assessed by varying the factorization and renormalization scales up and down by a factor of two from their nominal values.

The uncertainty on the integrated luminosity of 3.6% is derived, following the same methodology as that detailed in Ref. [89], from a preliminary calibration of the luminosity scale derived from beam-separation scans performed in April 2012. The uncertainties on the cross sections for $t\bar{t}$ +W and $t\bar{t}$ +Z are taken to be 50%, motivated by the cross section uncertainty in Ref. [55] and additional uncertainties on kinematic distributions evaluated with MADGRAPH+PYTHIA. The uncertainty on the cross section for W production in association with heavy flavor jets is taken from Ref. [90].

The uncertainty in the signal cross section is taken from an envelope of cross section predictions using different PDF sets (including the α_{S} uncertainty) and factorization and renormalization scales, as described in Ref. [62].

The background in the signal region and the impact of systematic uncertainties on the background yields and signal estimates are estimated with a fit based on the profile likelihood method [91]. The inputs to the fit are as follows:

1. The observed number of events in the semi-leptonic $t\bar{t}$ control region and the number expected from initial background estimates.

2. Transfer factors (TF) which are multiplicative factors that propagate the event count from the semi-leptonic $t\bar{t}$ control regions to the signal regions.

3. Background estimates in the signal region for Z+jets, multijets and fully-hadronic $t\bar{t}$ obtained as described in Sec. 6.

4. Expectations from simulation for the number of events from the remaining backgrounds ($t\bar{t}$ +boson, W+jets, single-top, diboson) in the signal regions.

The event count in each of the three control and three signal regions is treated with a Poisson probability density function. The statistical and systematic uncertainties on the expected yields are included in the probability density function as nuisance parameters, constrained to be Gaussian with a width given by the size of the uncertainty. Seventeen nuisance parameters are included in the fit. Correlations in the nuisance parameters from the $t\bar{t}$ control region to the signal region are taken into account where necessary. The Poisson probability density functions also includes a free parameter to scale the expected contribution from the semi-leptonic $t\bar{t}$ background in its control region. A likelihood is formed as the product of these probability density functions and the constraints on the nuisance parameters. The one free parameter and the nuisance parameters are adjusted to maximize the likelihood.

8 Results and interpretation

The predicted background in the signal regions and the observed numbers of events are shown in Table 2. No significant discrepancy is seen between the observed yields and SM expectations.

Number of events	**SR1**	**SR2**	**SR3**
Observed	15	2	1
Expected background	17.5 ± 3.2	4.7 ± 1.5	2.7 ± 1.2
Expected $t\bar{t}$	9.8 ± 2.6	1.9 ± 1.3	0.9 ± 0.7
Expected $t\bar{t}$ + W/Z	1.7 ± 1.0	0.7 ± 0.4	0.51 ± 0.30
Expected Z+jets	2.1 ± 1.0	1.2 ± 0.5	0.8 ± 0.4
Expected W+jets	1.2 ± 0.8	0.32 ± 0.29	$0.19^{+0.23}_{-0.19}$
Expected single-top	1.5 ± 0.9	0.5 ± 0.4	$0.3^{+0.5}_{-0.3}$
Expected multijet	0.12 ± 0.12	0.01 ± 0.01	< 0.01
Expected diboson	1.2 ± 1.2	< 0.22	< 0.22
Fit input expectation $t\bar{t}$	9.9	1.7	0.6

Table 2: The observed numbers of events in the three signal regions, and the background expectations. The input to the fit for the semi-leptonic $t\bar{t}$ background is also shown. The uncertainties shown are the statistical plus systematic uncertainties on the mean of the Poisson function describing the background probability density. Uncertainties on the inputs are not shown as they are almost the same as the uncertainties from the fit. Numerical rounding can cause the sum of the individual backgrounds to not add up exactly to the total.

The systematic uncertainty on the background ranges between 18% and 45% across the three signal regions. Significant contributions to this uncertainty arise from the theoretical

modeling of the main background processes, the jet energy scale/resolution and the limited number of events in the signal region for the background simulation samples. The dominant sources of systematic uncertainty are summarized in Table 3.

Uncertainty	**SR1**	**SR2**	**SR3**
Total	18%	33%	45%
Background sample sizes (data and simulation)	10%	17%	21%
Jet energy scale and resolution	10%	10%	25%
$t\bar{t}$ theory	10%	19%	22%
Z+jets theory	4%	8%	8%
$t\bar{t}+W/Z$ theory	5%	8%	10%

Table 3: The total systematic uncertainty on the background in each of the three signal regions and a list of the dominant contributions to the uncertainty. The individual uncertainties can be correlated.

For the signal prediction, the systematic uncertainty is approximately 30%, constant across the plane of top squark and LSP masses. The uncertainty is dominated by the uncertainties on the jet energy scale (25%) and b-tagging (15%) as well as by the theoretical uncertainties on the cross section (14%).

The distributions of $E_{\mathrm{T}}^{\mathrm{miss}}$ and $m_{\mathrm{T}}(b, E_{\mathrm{T}}^{\mathrm{miss}})$ are shown in Figure 4; in each of these distributions, all signal selection requirements have been applied except for the one on the variable being plotted. For the $m_{\mathrm{T}}(b, E_{\mathrm{T}}^{\mathrm{miss}})$ distribution, the $E_{\mathrm{T}}^{\mathrm{miss}}$ requirement is set to that of SR1 ($E_{\mathrm{T}}^{\mathrm{miss}} > 200$ GeV). The SM expectation shown is based on the initial normalization of the background contributions.

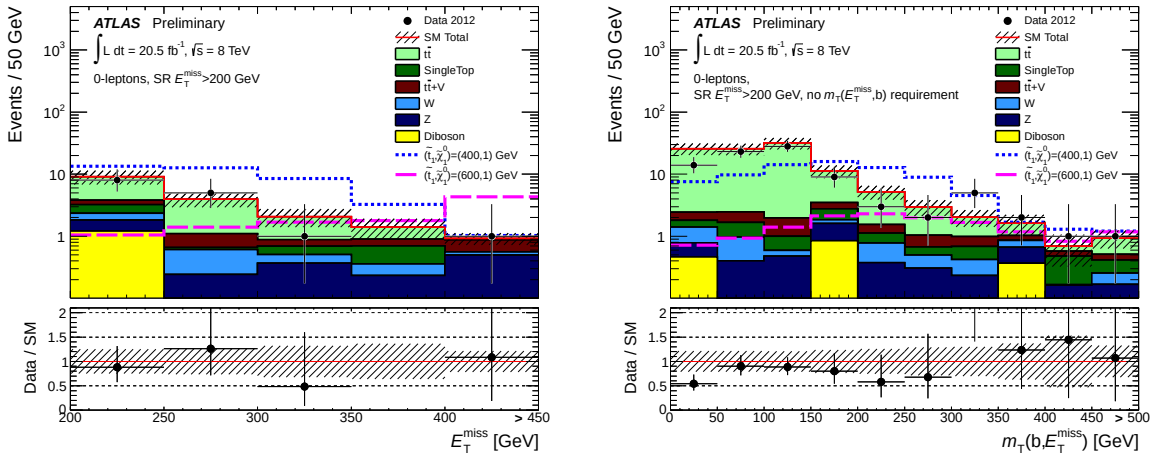

Figure 4: Distributions of $E_{\mathrm{T}}^{\mathrm{miss}}$ (left) and $m_{\mathrm{T}}(b, E_{\mathrm{T}}^{\mathrm{miss}})$ (right) after all selection requirements except for the one on the variable being plotted. The rightmost bin includes all overflows. For the $m_{\mathrm{T}}(b, E_{\mathrm{T}}^{\mathrm{miss}})$ distribution, $E_{\mathrm{T}}^{\mathrm{miss}} > 200$ GeV has been applied. The SM expectation shown here is the input to the SM background fit. The uncertainty band around the SM expectation combines statistical and systematic uncertainties.

Signal region	$\langle \varepsilon\sigma \rangle^{95}_{\text{obs}}$[fb]	S^{95}_{obs}	S^{95}_{exp}	CL_B
SR1	0.49	10.0	$10.6^{+5.5}_{-1.7}$	0.39
SR2	0.17	3.6	$5.3^{+3.2}_{-1.7}$	0.20
SR3	0.19	3.9	$4.5^{+1.9}_{-0.7}$	0.27

Table 4: Left to right: 95% CL upper limits on the visible cross section ($\langle \varepsilon\sigma \rangle^{95}_{\text{obs}}$) in the various signal regions, and on the number of signal events (S^{95}_{obs}). The third column (S^{95}_{exp}) shows the 95% CL upper limit on the number of signal events, given the expected number (and $\pm 1\sigma$ uncertainty on the expectation) of background events. The last column indicates the CL_B value, i.e. the observed confidence level for the background-only hypothesis.

Limits on the visible cross section (i.e. the cross section evaluated inside a given signal region) are obtained by including the number of events observed in that signal region as an input to the fit and deriving an additional parameter, representing the non-SM signal strength (constrained to be non-negative), as the output of the fit. Limits on the number of non-SM events in the signal region, obtained using the CL_s [92] prescription, are divided by the integrated luminosity to derive the constraints on the visible cross section. The limits at 95% confidence level (CL) are shown in Table 4.

For excluding specific models of new physics, the fit in the signal region proceeds in the same way. Limits are set in a model of direct top squark pair production, followed by top squark decay (with 100% branching ratio) to a top quark and the LSP ($pp \to \tilde{t}_1\tilde{t}_1^* \to t\tilde{\chi}_1^0\bar{t}\tilde{\chi}_1^0$). The limits in the plane of the masses of the top squark and LSP are shown in Fig. 5. For each pair of top squark and LSP masses, the signal region with the best expected sensitivity is used to set the limit. Top squarks in this model with masses between 320 and 660 GeV are excluded at 95% CL for a nearly massless LSP. For a LSP mass of 150 GeV the exclusion interval is between 400 and 620 GeV. These quoted values are obtained by taking a signal cross section that is lower than the nominal value by 1σ in the theoretical uncertainty. The difference in acceptance for top squarks corresponding to left-handed top quarks, compared to those in the (right-handed) model shown here are modest; the relative difference in acceptance is typically within 10%.

The results can also be used to derive upper limits on the branching ratio for $\tilde{t}_1 \to t\tilde{\chi}_1^0$ as a function of the masses of the top squark and LSP. The results are shown in Fig. 6. The conservative assumption is made here that this analysis has no sensitivity to other decay modes of the top squark. The nominal values for the signal cross sections are used to derive these branching ratio limits.

9 Conclusions

A search with the ATLAS detector for direct pair production of top squarks in final states containing six or more jets and $E_{\text{T}}^{\text{miss}}$ has been presented. Data from the full 2012 data-taking period, corresponding to an integrated luminosity of 20.5 fb^{-1}, at a pp center of mass energy of $\sqrt{s} = 8$ TeV, have been analyzed. Observations are consistent with SM expectations and exclusion limits have been placed in a model of top squark pair production, followed by the decay $\tilde{t}_1 \to t\tilde{\chi}_1^0$. Top squarks in this model with masses between 320 and 660 GeV are excluded at 95% CL for a nearly massless LSP. For a LSP mass of 150 GeV the exclusion interval is between 400

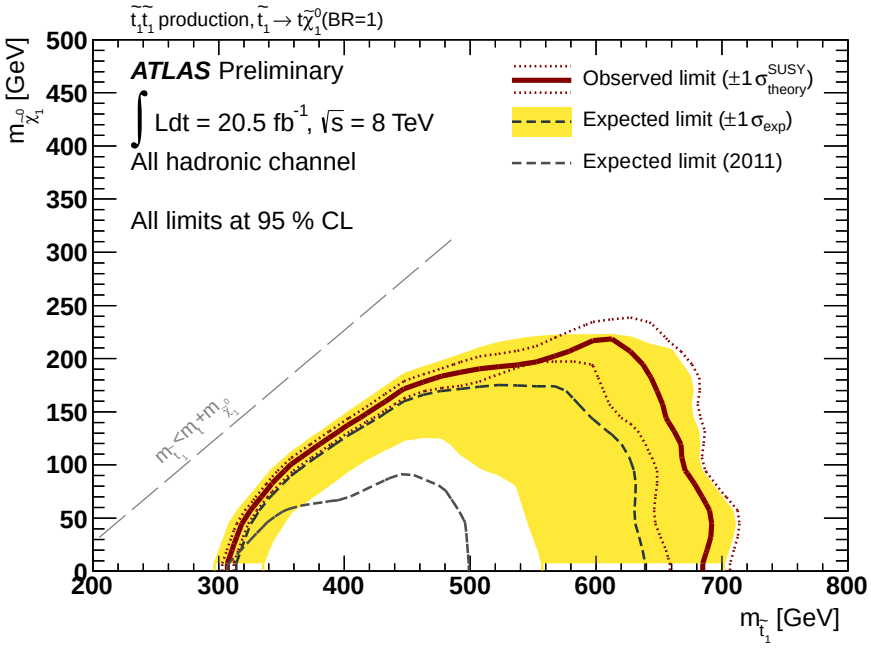

Figure 5: Expected and observed exclusion limits at 95% *CL* for the model of ($pp \to \tilde{t}_1\tilde{t}_1^* \to t\tilde{\chi}_1^0\bar{t}\tilde{\chi}_1^0$) with 100% branching ratio of $\tilde{t}_1 \to t\tilde{\chi}_1^0$. The top quark produced in the decay has a right-handed polarization in 95% of the decays. The band around the median expected limit shows the $\pm 1\sigma$ variations on the median expected limit, including all uncertainties except theoretical uncertainties on the signal. The dotted lines around the observed limit indicate the sensitivity to $\pm 1\sigma$ variations on these theoretical uncertainties. The expected limit from the previous ATLAS search [29] with the same final state is also shown.

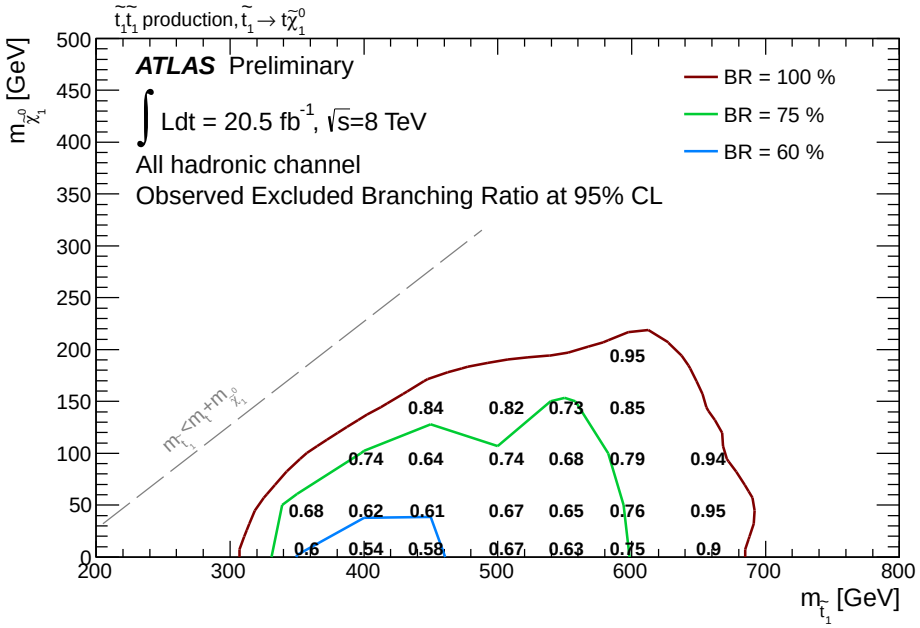

Figure 6: Excluded (at 95% *CL*) branching fractions for $\tilde{t}_1 \to t\tilde{\chi}_1^0$ in the model where $pp \to \tilde{t}_1\tilde{t}_1^*$. The conservative assumption is made here that this analysis is sensitive only to the decay channel $\tilde{t}_1 \to t\tilde{\chi}_1^0$ and has no sensitivity to other decay modes.

and 620 GeV. The result significantly extends previous limits in the all-hadronic final state and excludes top squarks up to higher masses than in previous searches.

References

[1] L. Evans and P. Bryant, *LHC Machine*, JINST **3** (2008) S08001.

[2] ATLAS Collaboration, *Observation of a new particle in the search for the Standard Model Higgs boson with the ATLAS detector at the LHC*, Phys.Lett. **B716** (2012) 1–29, arXiv:1207.7214 [hep-ex].

[3] CMS Collaboration, *Observation of a new boson at a mass of 125 GeV with the CMS experiment at the LHC*, Phys.Lett. **B716** (2012) 30–61, arXiv:1207.7235 [hep-ex].

[4] S. Weinberg, *Implications of Dynamical Symmetry Breaking*, Phys. Rev. **D13** (1976) 974–996.

[5] E. Gildener, *Gauge Symmetry Hierarchies*, Phys. Rev. **D14** (1976) 1667.

[6] S. Weinberg, *Implications of Dynamical Symmetry Breaking: An Addendum*, Phys. Rev. **D19** (1979) 1277–1280.

[7] L. Susskind, *Dynamics of Spontaneous Symmetry Breaking in the Weinberg- Salam Theory*, Phys. Rev. **D20** (1979) 2619–2625.

[8] H. Miyazawa, *Baryon Number Changing Currents*, Prog. Theor. Phys. **36 (6)** (1966) 1266–1276.

[9] P. Ramond, *Dual Theory for Free Fermions*, Phys. Rev. **D3** (1971) 2415–2418.

[10] Y. Golfand and E. Likhtman, *Extension of the Algebra of Poincare Group Generators and Violation of p Invariance*, JETP Lett. **13** (1971) 323–326.

[11] A. Neveu and J. H. Schwarz, *Factorizable dual model of pions*, Nucl. Phys. **B31** (1971) 86–112.

[12] A. Neveu and J. H. Schwarz, *Quark Model of Dual Pions*, Phys. Rev. **D4** (1971) 1109–1111.

[13] J. Gervais and B. Sakita, *Field theory interpretation of supergauges in dual models*, Nucl. Phys. **B34** (1971) 632–639.

[14] D. Volkov and V. Akulov, *Is the Neutrino a Goldstone Particle?*, Phys. Lett. **B46** (1973) 109–110.

[15] J. Wess and B. Zumino, *A Lagrangian Model Invariant Under Supergauge Transformations*, Phys. Lett. **B49** (1974) 52.

[16] J. Wess and B. Zumino, *Supergauge Transformations in Four-Dimensions*, Nucl. Phys. **B70** (1974) 39–50.

[17] S. Dimopoulos and H. Georgi, *Softly Broken Supersymmetry and SU(5)*, Nucl. Phys. **B193** (1981) 150.

[18] E. Witten, *Dynamical Breaking of Supersymmetry*, Nucl. Phys. **B188** (1981) 513.

[19] M. Dine, W. Fischler, and M. Srednicki, *Supersymmetric Technicolor*, Nucl. Phys. **B189** (1981) 575–593.

[20] S. Dimopoulos and S. Raby, *Supercolor*, Nucl. Phys. **B192** (1981) 353.

[21] N. Sakai, *Naturalness in Supersymmetric Guts*, Z. Phys. **C11** (1981) 153.

[22] R. Kaul and P. Majumdar, *Cancellation of quadratrically divergent mass corrections in globally supersymmetric spontaneously broken gauge theories*, Nucl. Phys. **B199** (1982) 36.

[23] R. Barbieri and G. Giudice, *Upper Bounds on Supersymmetric Particle Masses*, Nucl.Phys. **B306** (1988) 63.

[24] B. de Carlos and J. Casas, *One loop analysis of the electroweak breaking in supersymmetric models and the fine tuning problem*, Phys.Lett. **B309** (1993) 320–328, arXiv:hep-ph/9303291 [hep-ph].

[25] P. Fayet, *Supersymmetry and Weak, Electromagnetic and Strong Interactions*, Phys. Lett. **B64** (1976) 159.

[26] P. Fayet, *Spontaneously Broken Supersymmetric Theories of Weak, Electromagnetic and Strong Interactions*, Phys. Lett. **B69** (1977) 489.

[27] G. R. Farrar and P. Fayet, *Phenomenology of the Production, Decay, and Detection of New Hadronic States Associated with Supersymmetry*, Phys. Lett. **B76** (1978) 575–579.

[28] P. Fayet, *Relations Between the Masses of the Superpartners of Leptons and Quarks, the Goldstino Couplings and the Neutral Currents*, Phys. Lett. **B84** (1979) 416.

[29] ATLAS Collaboration, *Search for a supersymmetric partner to the top quark in final states with jets and missing transverse momentum at* $\sqrt{s} = 7$ *TeV with the ATLAS detector*, Phys. Rev. Lett. **109** (2012) 211802, arXiv:1208.1447 [hep-ex].

[30] ATLAS Collaboration, *Search for direct stop production in events with missing transverse momentum and two b-jets using 12.8* fb^{-1} *of pp collisions at* $\sqrt{s} = 8$ *TeV with the ATLAS detector*, ATLAS-CONF-2013-001 (2013). http://cds.cern.ch/record/1503233.

[31] ATLAS Collaboration, *Search for direct top squark pair production in final states with one isolated lepton, jets, and missing transverse momentum in* $\sqrt{s} = 8$ *TeV pp collisions using 13.0* fb^{-1} *of ATLAS data*, ATLAS-CONF-2012-166 (2012). http://cds.cern.ch/record/1497732.

[32] ATLAS Collaboration, *Search for light top squark pair production in final states with leptons and b-jets with the ATLAS detector in* $\sqrt{s} = 7$ *TeV proton-proton collisions*, arXiv:1209.2102 [hep-ex].

[33] ATLAS Collaboration, *Search for light scalar top quark pair production in final states with two leptons with the ATLAS detector in* $\sqrt{s} = 7$ *TeV proton-proton collisions*, Eur. Phys. J. **C72** (2012) 2237, arXiv:1208.4305 [hep-ex].

[34] ATLAS Collaboration, *Search for scalar top quark pair production in natural gauge mediated supersymmetry models with the ATLAS detector in* pp *collisions at* $\sqrt{s} = 7$ *TeV*, Phys.Lett. **B715** (2012) 44–60, arXiv:1204.6736 [hep-ex].

[35] CMS Collaboration, *Search for direct top squark pair production in events with a single isolated lepton, jets and missing transverse energy at* $\sqrt{s} = 8$ *TeV*, CMS-PAS-SUS-12-023 (2012). http://cds.cern.ch/record/1494074.

[36] CMS Collaboration, *Inclusive search for supersymmetry using the razor variables in pp collisions at $\sqrt{s} = 7$ TeV*, arXiv:1212.6961 [hep-ex].

[37] CMS Collaboration, *Search for supersymmetry in final states with missing transverse energy and 0, 1, 2, or at least 3 b-quark jets in 7 TeV pp collisions using the variable alphaT*, JHEP **1301** (2013) 077, arXiv:1210.8115 [hep-ex].

[38] CMS Collaboration, *Scalar Top Quark Search with Jets and Missing Momentum in pp Collisions at $\sqrt{s} = 7$ TeV*, CMS-PAS-SUS-11-030 (2011). http://cds.cern.ch/record/1494575.

[39] S. Frixione, P. Nason, and C. Oleari, *Matching NLO QCD computations with Parton Shower simulations: the POWHEG method*, JHEP **0711** (2007) 070, arXiv:0709.2092 [hep-ph].

[40] S. Frixione and B. R. Webber, *Matching NLO QCD computations and parton shower simulations*, JHEP **0206** (2002) 029, arXiv:hep-ph/0204244 [hep-ph].

[41] S. Frixione, E. Laenen, P. Motylinski, and B. R. Webber, *Single-top production in MC@NLO*, JHEP **0603** (2006) 092, arXiv:hep-ph/0512250 [hep-ph].

[42] B. P. Kersevan and E. Richter-Was, *The Monte Carlo event generator AcerMC version 2.0 with interfaces to PYTHIA 6.2 and HERWIG 6.5*, arXiv:hep-ph/0405247 [hep-ph].

[43] T. Gleisberg et al., *Event generation with SHERPA 1.1*, JHEP **0902** (2009) 007, arXiv:0811.4622 [hep-ph].

[44] J. Alwall et al., *MadGraph 5 : Going Beyond*, JHEP **1106** (2011) 128, arXiv:1106.0522 [hep-ph].

[45] G. Corcella et al., *HERWIG 6.5 release note*, arXiv:hep-ph/0210213 [hep-ph].

[46] J. Butterworth, J. R. Forshaw, and M. Seymour, *Multiparton interactions in photoproduction at HERA*, Z. Phys. **C72** (1996) 637–646.

[47] T. Sjöstrand, S. Mrenna, and P. Z. Skands, *PYTHIA 6.4 Physics and Manual*, JHEP **0605** (2006) 026, arXiv:hep-ph/0603175 [hep-ph].

[48] H.-L. Lai et al., *New parton distributions for collider physics*, Phys. Rev. **D82** (2010) 074024, arXiv:1007.2241 [hep-ph].

[49] J. Pumplin et al., *New generation of parton distributions with uncertainties from global QCD analysis*, JHEP **0207** (2002) 012, arXiv:hep-ph/0201195 [hep-ph].

[50] ATLAS Collaboration, *ATLAS tunes of PYTHIA 6 and Pythia 8 for MC11*, ATL-PHYS-PUB-2011-009 (2011). http://cds.cern.ch/record/1363300.

[51] ATLAS Collaboration, *New ATLAS event generator tunes to 2010 data*, ATL-PHYS-PUB-2011-008 (2011). http://cds.cern.ch/record/1345343.

[52] S. Catani et al., *Vector boson production at hadron colliders: A Fully exclusive QCD calculation at NNLO*, Phys.Rev.Lett. **103** (2009) 082001, arXiv:0903.2120 [hep-ph].

[53] A. Martin, W. Stirling, R. Thorne, and G. Watt, *Parton distributions for the LHC*, Eur.Phys.J. **C63** (2009) 189–285, arXiv:0901.0002 [hep-ph].

[54] M. Aliev et al., *HATHOR: HAdronic Top and Heavy quarks crOss section calculatoR*, Comput. Phys. Commun. **182** (2011) 1034, arXiv:1007.1327 [hep-ph].

[55] J. M. Campbell and R. K. Ellis, *$t\bar{t}W^{+-}$ production and decay at NLO*, JHEP **1207** (2012) 052, arXiv:1204.5678 [hep-ph].

[56] M. Garzelli, A. Kardos, C. Papadopoulos, and Z. Trocsanyi, *Z^0 - boson production in association with a top anti-top pair at NLO accuracy with parton shower effects*, Phys.Rev. **D85** (2012) 074022, arXiv:1111.1444 [hep-ph].

[57] J. M. Campbell, R. K. Ellis, and C. Williams, *Vector boson pair production at the LHC*, JHEP **1107** (2011) 018, arXiv:1105.0020 [hep-ph].

[58] M. Bähr et al., *Herwig++ Physics and Manual*, Eur. Phys. J. **C58** (2008) 639–707, arXiv:0803.0883 [hep-ph].

[59] W. Beenakker et al., *Stop production at hadron colliders*, Nucl. Phys. **B515** (1998) 3–14.

[60] W. Beenakker et al., *Supersymmetric top and bottom squark production at hadron colliders*, JHEP **1008** (2010) 098, arXiv:1006.4771 [hep-ph].

[61] W. Beenakker et al., *Squark and gluino hadroproduction*, Int. J. Mod. Phys. **A26** (2011) 2637–2664.

[62] M. Krämer et al., *Supersymmetry production cross sections in pp collisions at sqrt(s) = 7 TeV*, arXiv:1206.2892 [hep-ph] (2012), arXiv:1206.2892 [hep-ph].

[63] ATLAS Collaboration, *The ATLAS Simulation Infrastructure*, Eur. Phys. J. **C70** (2010) 823–874.

[64] GEANT4 Collaboration, S. Agostinelli et al., *GEANT4: A simulation toolkit*, Nucl. Instrum. Meth. **A506** (2003) 250–303.

[65] ATLAS Collaboration, *The simulation principle and performance of the ATLAS fast calorimeter simulation FastCaloSim*, ATL-PHYS-PUB-2010-013 (2010). http://cds.cern.ch/record/1300517.

[66] ATLAS Collaboration, *The ATLAS Experiment at the CERN Large Hadron Collider*, JINST **3** (2008) S08003.

[67] ATLAS Collaboration, *Expected Performance of the ATLAS Experiment - Detector, Trigger and Physics*, CERN-OPEN-2008-020, arXiv:0901.0512 [hep-ex].

[68] ATLAS Collaboration, *Performance of primary vertex reconstruction in proton-proton collisions at $\sqrt{s}$ = 7 TeV in the ATLAS experiment*, ATLAS-CONF-2010-069 (2010). http://cdsweb.cern.ch/record/1281344.

[69] ATLAS Collaboration, *Electron performance measurements with the ATLAS detector using the 2010 LHC proton-proton collision data*, Eur. Phys. J. **C72** (2012) 1909, arXiv:1110.3174 [hep-ex].

[70] ATLAS Collaboration, *A measurement of the ATLAS muon reconstruction and trigger efficiency using J/psi decays*, ATLAS-CONF-2011-021 (2011). http://cdsweb.cern.ch/record/1336750.

[71] ATLAS Collaboration, *Muon reconstruction efficiency in reprocessed 2010 LHC proton-proton collision data recorded with the ATLAS detector*, ATLAS-CONF-2011-063 (2011). http://cdsweb.cern.ch/record/1345743.

[72] M. Cacciari, G. P. Salam, and G. Soyez, *The Anti-k(t) jet clustering algorithm*, JHEP **0804** (2008) 063, arXiv:0802.1189 [hep-ph].

[73] M. Cacciari and G. P. Salam, *Dispelling the N^3 myth for the k_t jet-finder*, Phys. Lett. **B641** (2006) 57, arXiv:hep-ph/0512210.

[74] ATLAS Collaboration, *Jet energy measurement with the ATLAS detector in proton-proton collisions at sqrt(s) = 7 TeV*, arXiv:1112.6426 [hep-ex]. Submitted to Eur. Phys. J. C.

[75] ATLAS Collaboration, *Performance of missing transverse momentum reconstruction in proton-proton collisions at 7 TeV with ATLAS*, Eur. Phys. J. **C72** (2012) 1844, arXiv:1108.5602 [hep-ex].

[76] ATLAS Collaboration, *Measurement of the b-tag Efficiency in a Sample of Jets Containing Muons with 5 fb^{-1} of Data from the ATLAS Detector*, ATLAS-CONF-2012-043 (2012). http://cdsweb.cern.ch/record/1435197.

[77] ATLAS Collaboration, *Calibrating the b-Tag Efficiency and Mistag Rate in 35 pb^{-1} of Data with the ATLAS Detector*, ATLAS-CONF-2011-089 (2011). http://cdsweb.cern.ch/record/1356198.

[78] ATLAS Collaboration, *Commissioning of the ATLAS high-performance b-tagging algorithms in the 7 TeV collision data*, ATLAS-CONF-2011-102 (2011). http://cdsweb.cern.ch/record/1369219.

[79] ATLAS Collaboration, *Selection of jets produced in proton-proton collisions with the ATLAS detector using 2011 data*, ATLAS-CONF-2012-020 (2012). http://cdsweb.cern.ch/record/1430034.

[80] ATLAS Collaboration, *Studies of the performance of the ATLAS detector using cosmic-ray muons*, Eur.Phys.J. **C71** (2011) 1593, arXiv:1011.6665 [physics.ins-det].

[81] T. Sjöstrand, S. Mrenna, and P. Z. Skands, *A Brief Introduction to PYTHIA 8.1*, Comput.Phys.Commun. **178** (2008) 852–867, arXiv:0710.3820 [hep-ph].

[82] ATLAS Collaboration, *Search for squarks and gluinos with the ATLAS detector in final states with jets and missing transverse momentum using 4.7 fb^{-1} of $\sqrt{s} = 7$ TeV proton-proton collision data*, Phys. Rev. D **87** (2013) 012008, arXiv:1208.0949 [hep-ex].

[83] ATLAS Collaboration, *Jet energy scale and its systematic uncertainty in prroton-proton collisions at $\sqrt{s} = 7$ TeV with ATLAS 2011 data*, ATLAS-CONF-2013-004 (2013). http://cdsweb.cern.ch/record/1509552.

[84] D0 Collaboration, V. Abazov et al., *b-Jet Identification in the D0 Experiment*, Nucl. Instrum. Meth. **A620** (2010) 490, arXiv:1002.4224 [hep-ex].

[85] ATLAS Collaboration, *b-Jet Tagging Efficiency Calibration using the System8 Method*, ATLAS-CONF-2011-143 (2011). http://cdsweb.cern.ch/record/1386703.

[86] ATLAS Collaboration, *Measurement of the Mistag Rate of b-tagging algorithms with 5 fb^{-1} of Data Collected by the ATLAS Detector*, ATLAS-CONF-2012-040 (2012). http://cdsweb.cern.ch/record/1435194.

[87] ATLAS Collaboration, *b-jet tagging calibration on c-jets containing D^{*+} mesons*, ATLAS-CONF-2012-039 (2012). http://cdsweb.cern.ch/record/1435193.

[88] ATLAS Collaboration, *Measurement of $t\bar{t}$ production with a veto on additional central jet activity in pp collisions at sqrt(s) = 7 TeV using the ATLAS detector*, Eur.Phys.J. **C72** (2012) 2043, arXiv:1203.5015 [hep-ex].

[89] ATLAS Collaboration, *Improved luminosity determination in pp collisions at sqrt(s) = 7 TeV using the ATLAS detector at the LHC*, arXiv:1302.4393 [hep-ex].

[90] ATLAS Collaboration, *Measurement of the charge asymmetry in top quark pair production in pp collisions at sqrt(s) = 7 TeV using the ATLAS detector*, Eur. Phys. J. **C72** (2012) 2039, arXiv:1203.4211 [hep-ex].

[91] G. Cowan, K. Cranmer, E. Gross, and O. Vitells, *Asymptotic formulae for likelihood-based tests of new physics*, Eur. Phys. J. **C71** (2011) 1554, arXiv:1007.1727 [physics.data-an].

[92] A. L. Read, *Presentation of search results: The CL(s) technique*, J. Phys. **G28** (2002) 2693.

A Additional information on signal models and interpretations

The number of events surviving after the successive application of selection requirements is shown in Table 5 for the signal model consisting of a 600 GeV top squark and a massless LSP. The numbers are shown for two models of $pp \to \tilde{t}_1\tilde{t}_1^* \to t\tilde{\chi}_1^0\bar{t}\tilde{\chi}_1^0$. In the left (right) column, the top squark decays to a top quark with a right-handed (left-handed) polarization in 95% (100%) of the decays.

Selection	$\tilde{t}_R\tilde{t}_R^*$	$\tilde{t}_L\tilde{t}_L^*$
No selection	507.3	507.3
Trigger	468.0	467.8
Primary Vertex	467.8	467.4
Event cleaning	459.0	459.6
Muon veto	381.2	382.5
Electron veto	284.4	292.3
$E_{\mathrm{T}}^{\mathrm{miss}} > 130$ GeV	263.1	270.1
Jet multiplicity and p_{T}	97.7	92.2
$E_{\mathrm{T}}^{\mathrm{miss,track}} > 30$ GeV	96.3	90.5
$\Delta\phi(E_{\mathrm{T}}^{\mathrm{miss}}, E_{\mathrm{T}}^{\mathrm{miss,track}}) < \pi/3$	90.3	84.3
$\Delta\phi(\mathrm{jet}, \mathrm{E}_{\mathrm{T}}^{\mathrm{miss}}) > \pi/5$	77.1	72.0
Tau veto	67.4	61.9
≥ 2 b-tagged jets	29.5	31.5
$m_{\mathrm{T}}(b\text{-jet}, E_{\mathrm{T}}^{\mathrm{miss}}) > 175$ GeV	20.2	23.6
80 GeV$< m_{jjj}^0 <$ 270 GeV	17.8	20.4
80 GeV$< m_{jjj}^1 <$ 270 GeV	10.9	11.9
$E_{\mathrm{T}}^{\mathrm{miss}} > 150$ GeV	10.8	11.8
$E_{\mathrm{T}}^{\mathrm{miss}} > 200$ GeV	10.3	11.2
$E_{\mathrm{T}}^{\mathrm{miss}} > 250$ GeV	9.2	10.0
$E_{\mathrm{T}}^{\mathrm{miss}} > 300$ GeV	7.8	8.3
$E_{\mathrm{T}}^{\mathrm{miss}} > 350$ GeV	6.1	6.6

Table 5: Weighted number of events surviving after the successive application of selection requirements for the signal model consisting of a 600 GeV top squark and a massless LSP. The numbers are shown for the cases where the top squark is the partner of the right-handed (left-handed) top quark. The numbers have been normalized to an integrated luminosity of 20.5 fb^{-1}. Additional weights have been applied to account for differences between data and simulation for the lepton trigger and reconstruction efficiencies, momentum scale and resolution, and for the efficiency and mis-tag rates for b-quark tagging. The raw number of events is 250000 before any selection requirements.

The signal region giving the best expected sensitivity as a function of the masses of the top squark and LSP is shown in Fig. 7.

The limits in the plane of the masses of the top squark and LSP are shown in Fig. 8. The numbers indicate the signal cross section in pb excluded at 95% *CL*.

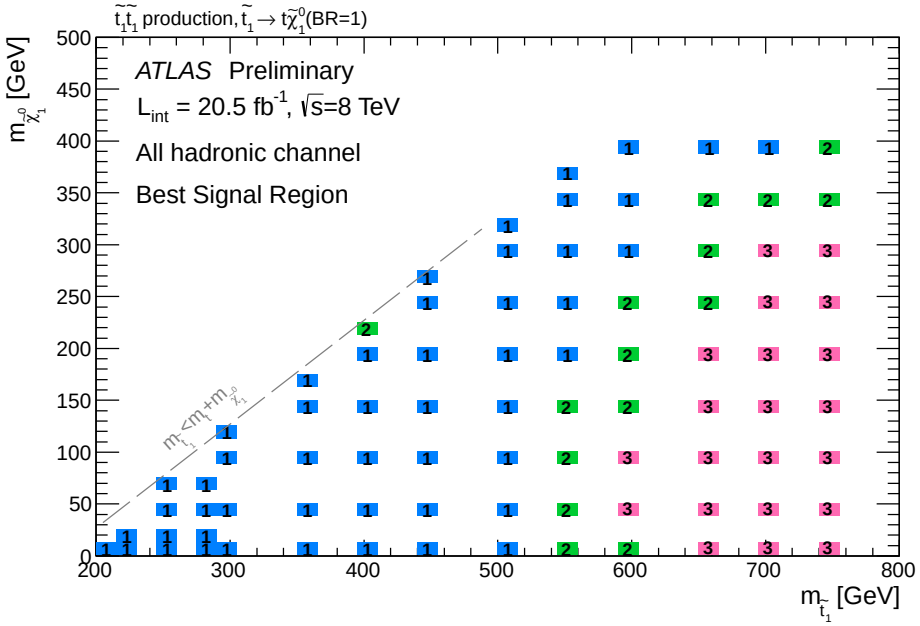

Figure 7: The signal region giving the best expected sensitivity as a function of the masses of the top squark and LSP in the model of ($pp \to \tilde{t}_1\tilde{t}_1^* \to t\tilde{\chi}_1^0\bar{t}\tilde{\chi}_1^0$) with 100% branching ratio of $\tilde{t}_1 \to t\tilde{\chi}_1^0$. The numbers (1,2,3) and colors (blue,green,pink) correspond to the three signal regions: SR1, SR2 and SR3.

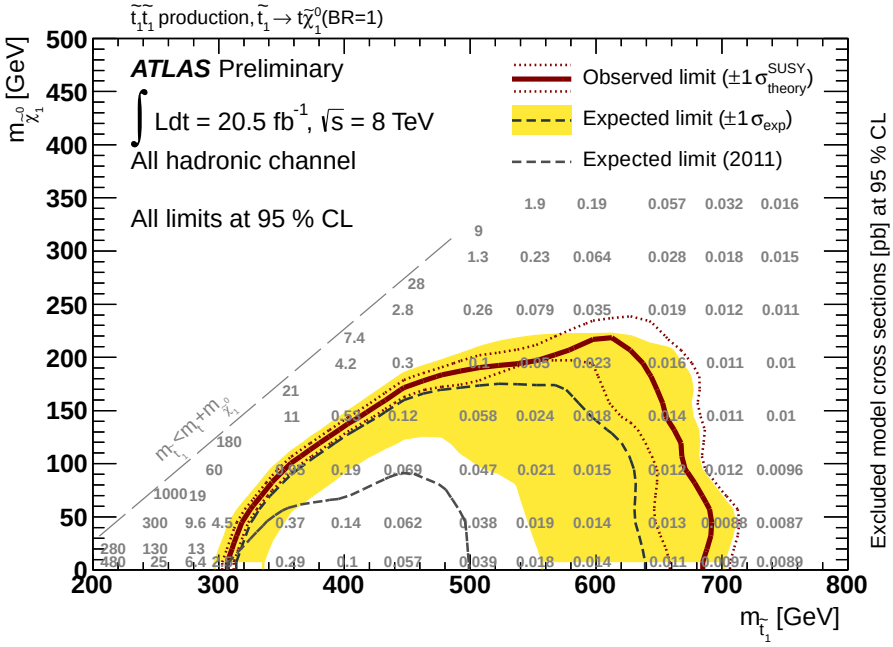

Figure 8: Expected and observed exclusion limits at 95% *CL* for the model of ($pp \to \tilde{t}_1\tilde{t}_1^* \to t\tilde{\chi}_1^0\bar{t}\tilde{\chi}_1^0$) with 100% branching ratio of $\tilde{t}_1 \to t\tilde{\chi}_1^0$. The band around the median expected limit shows the $\pm1\sigma$ variations on the median expected limit, including all uncertainties except theoretical uncertainties on the signal. The dotted lines around the observed limit indicate the sensitivity to $\pm1\sigma$ variations on these theoretical uncertainties. The numbers indicate the signal cross section in pb excluded at 95% *CL*. The expected limit from the previous ATLAS search [29] with the same final state is also shown.